CALPHAD: Computer Coupling of Phase Diagrams and Thermochemistry 51 (2015) 252–260

Contents lists available at ScienceDirect

CALPHAD: Computer Coupling of Phase Diagrams and Thermochemistry

journal homepage: www.elsevier.com/locate/calphad

Thermodynamic assessment of the Al–Cu–Zn system, part II: Al–Cu binary system

Song-Mao Liang, Rainer Schmid-Fetzer *

Institute of Metallurgy, Clausthal University of Technology, D-38678 Clausthal-Zellerfeld, Germany

ARTICLE INFO

Article history:
Received 21 August 2015
Received in revised form
12 October 2015
Accepted 12 October 2015

Keywords:
Phase Equilibria
Thermodynamics
Calphad assessment
Al–Cu system

ABSTRACT

The thermodynamic description of the Al–Cu system is reassessed, and for the first time all available experimental data have been comprehensively compared with calculated results. Key distinctions from previous Calphad descriptions are worked out. The new model for the γ_1 and γ_2 phases partially reflects the crystal structure while being sufficiently simple for a realistic joining with the γ-CuZn phase in the Al–Cu–Zn ternary system. The η_1/η_2 phase transition and the α_2 phase have been introduced in the description for the first time. An improved agreement of the calculated phase diagram with experimental data, very good agreement with the extensive thermodynamic properties of the liquid phase and reasonable agreement for solid phase thermodynamic properties is demonstrated.

© 2015 Elsevier Ltd. All rights reserved.

1. Introduction

The thermodynamic description of the Al–Cu system is essential for focused development of Al-based and Cu-based alloys. It is also a key binary edge system for Zn–Al–Cu ternary alloys and, as such, important for Zn-based alloys and thermodynamic databases. In the first thermodynamic description of Al–Cu system [1], four intermediate θ (Al_2Cu), η (AlCu), γ (Al_4Cu_9) and β (Bcc) phases were considered, and the θ, η and γ phases are treated as stoichiometric phases. Later, Murray [2] improved the thermodynamic description of [1] based on a review of the experimental work on Al–Cu system by 1985. Besides these four intermetallic phases, Chen et al. [3] introduced two more stoichiometric phases, the δ_1 and α_2 phases, into their thermodynamic modeling. Currently, it is the thermodynamic description of the Al–Cu system [4] offered in the public COST507 database that has been most widely used and accepted in multicomponent databases. Unfortunately, only the optimized parameters were published in the COST507 book [4]. Nothing is found on the experimental data evaluation, the thermodynamic model selection and, most importantly, the comparison of calculated results with experimental data for the Al–Cu system in the COST507 publication [4] or any later publication from that author. Based on that dataset [4], Liang and Chang [5] simplified the γ_1-Al_4Cu_9 (cP52, *P-43m*) phase from a three sublattice model to a single sublattice model together with the γ-Cu_8Zn_5 (cI52, *I-43m*) phase in the Cu–Zn system, thus obtaining a complete solid solution range of the γ phase in the Al–Cu–Zn ternary system. Miettinen [6] accepted all the models used as [5] and revised some parameters for their Cu–Al–Zn system. However, their thermodynamic description [6] only focused on the Cu-rich corner, and did not provide parameters for Al-rich phases. But if introducing the missing parameters from [4], then the calculated Al–Cu phase diagram in full composition range is completely off. Witusiewicz et al. [7] revised some parameters of the γ_1-Al_4Cu_9 phase and the liquid phase of [4] in order to avoid an artifact below room temperature and the temperature dependence of the liquid enthalpy of mixing in [4].

Although several thermodynamic descriptions of the Al–Cu binary system are available in the literature [1–7], none of them provided a comprehensive comparison between results of thermodynamic calculations and available experimental data. In addition, some new experimental results after 1991, the actual year of the COST507 assessment [4] also need to be taken into consideration. It is the purpose of this study to provide this thorough thermodynamic reassessment of the Al–Cu system, which will also serve as a key binary edge system of the Al–Cu–Zn ternary.

2. Critical review of experimental literature data

2.1. Crystal structure of solid phases

Table 1 [8–11] compiles the crystal structure information of all solid phases. The phase names used as Greek symbols in the text and in the TDB file of this work are provided in the first column.

* Corresponding author.
E-mail addresses: songmao.liang@tu-clausthal.de (S.-M. Liang), schmid-fetzer@tu-clausthal.de (R. Schmid-Fetzer).

http://dx.doi.org/10.1016/j.calphad.2015.10.004
0364-5916/© 2015 Elsevier Ltd. All rights reserved.

Table 1
Solid phases in the Al–Cu binary system.

Phase notation/Name in TDB [This work]	Sublattice model [This work]	Sublattice Model in [4,7]	Phase name/ Temperature range (°C)[a]	Pearson symbol/*Space group*/Prototype[a]	Maximum reported composition range (at%)[a]
(Al) Fcc	(Al,Cu)1	(Al,Cu)1	(Al) ≤ 660.45	cF4 *Fm-3m* Cu	0–2.48% Cu
(Cu) Fcc	(Al,Cu)1	(Al,Cu)1	(Cu) ≤ 1084.62	cF4 *Fm-3m* Cu	80.3–100% Cu
θ Al2Cu	(Al)2 (Al,Cu)1	(Al)2 (Al,Cu)1	θ, $CuAl_2$ ≤ 591	tI12 *I4/mcm* $CuAl_2$	31.9–33.0% Cu
η_1 Eta1	(Al,Cu)1 (Cu)1	(Al,Cu)1 (Cu)1	η_1, CuAl(h) 624-560	oS32[b] *Cmmm* $Cu_{0.94}$ $Al_{0.94}$	49.8–52.4% Cu
η_2 Eta2	(Al)48 (Cu)52	(Al,Cu)1 (Cu)1	η_2, CuAl(r) ≤ 561	mC20 *C2/m* CuAl(r)	49.8–52.3% Cu
ζ Al9Cu11	(Al,Cu)9 (Cu)11	(Al)9 (Cu)11	ζ_1, CuAl(h)[c] 590–530[a] Stable at 550 and 400 (10 days)[c]	oF88-4.7[c] *Fmm2* $Cu_{47.8}$ $Al_{35.5}$	55.2–59.8% Cu[a] Single phase 57.5% Cu (550 °C)[c]
ζ Al9Cu11	(Al,Cu)9 (Cu)11	(Al)9 (Cu)11	ζ_2, CuAl(r)[d] ≤ 570[a] Decomposes at 400 forming ζ_1 [d]	oI24-3.5[d] *Imm2* $Cu_{11.5}Al_{9.0}$	55.2–56.3% Cu 55–58% Cu[d] single phase 56.8% Cu [d]
ε_1 Bcc	(Al,Cu)1	(Al,Cu)1	ε_1, $Cu_{1-x}Al_x$ (958-848)	Cubic?	59.4–62.1% Cu
ε_2 Eps2	(Al,Cu)1 (Cu)1	(Al,Cu)1 (Cu)1	ε_2, $Cu_{2-x}Al$ (850-560)	hP6 *P6$_3$/mmc* Ni_2In (NiAs type)	55.0–61.1% Cu,
δ_1 Al5Cu8	(Al)5 (Cu)8	(Al)2 (Cu)3	δ, $Cu_{1-x}Al_x$	hR* R-3m	59.3–61.9% Cu
γ_2 Gam2	(Cu)2 (Cu)3 (Al,Cu)8	(Al)4 (Al,Cu)1 (Cu)8	γ_0, $Cu_{1-x}Al_x$ 1037-800	cI52 *I-43m* Cu_5Zn_8	59.8–69% Cu
γ_1 Gam1	(Cu)2 (Cu)3 (Al,Cu)8	(Al)4 (Al,Cu)1 (Cu)8	γ_1, Cu_9Al_4 < 890	cP52 *P-43m* Cu_9Al_4	62–68% Cu
β Bcc	(Al,Cu)1	(Al,Cu)1	β, Cu_3Al (h) 1049-559	cI2 *Im-3m*W	70.6–82.0% Cu
α_2 Alpha2	(Al)23 (Cu)77	–	α_2, $Cu_{1-x}Al_x$ < 363	($TiAl_3$ type)	76.5–78% Cu

[a] Data in the last three columns are generally from MSIT report [8] and accepted as assessment of experimental information.
[b] Crystal structure of η_1 is from [9].
[c] ζ_1 is perceived as high-temperature phase [2, 8], marked data are of from [11], notation (ζ_2/ζ_1) differs in [9].
[d] ζ_2 is perceived as low-temperature phase [2, 8], marked data are of from [10], notation (ζ_2/ζ_1) differs in [9].

For convenience, the corresponding phase names used in [2,8] are shown in column 4. The crystal structures of the solid phases are also generally accepted from the Materials Science International Team (MSIT) report [8]. Here we only present the experimental results published later than 2004 or not included in [8].

In the earlier review [2], the η_1 phase was reported as orthorhombic structure with Pearson symbol of oP16 and space group of *Pban* [12] or with Pearson symbol of oC16 and space group *Cmmm* from another unknown source. In [8], the η_1 phase is reported just as o*32. Recently, Ponweiser and Richter [9] determined the crystal structure of η_1–$CuAl_{1-\delta}$ phase as orthorhombic (space group *Cmmm*), their data are accepted here.

In [2], the high temperature stable ζ_1 phase was reported as hP42 with space group P6/mmm cited from [12], and the room temperature ζ_2 phase was possibly monoclinic cited from [13]. In the review [8], it is stated that the ζ_1 phase (*oF*88, *Fmm2*) is stable at temperature range from 530 to 590 °C, and the ζ_2 phase (*oI*24, *Imm2*) is stable at temperature below 570 °C, referring to a conference abstract [14]. However, in the work published later by the same group, Gulay and Harbrecht [10,11] reported that the ζ_1–Al_3Cu_4 (*oF*88, *Fmm2*) phase is stable at 400 °C and 550 °C [11], while the ζ_2–$Al_3Cu_{4-\delta}$ (*oI*24, *Imm2*) phase is stable at 530 °C but metastable at 400 °C [10]. At 450 °C, the mixture of ζ_1 and ζ_2 phases is seen, thus they proposed that the eutectoid decomposition temperature of ζ_1 into ζ_2 and η_1 is between 400 °C and 450 °C, and the ζ_2 phase is metastable at ambient temperature [10]. Since it is controversial to distinguish the ζ_1 and ζ_2 phase, we treat them as a single ζ phase for simplicity.

The α_2 phase is reported to form below 363 °C at about 77.5 at% Cu with an ordered Fcc long-period superlattice structure [2,8]. The α_2 phase is considered in this work as opposed to any previous Calphad assessment. Additional metastable phases are discussed in detail in the review [2].

2.2. Thermodynamic data

Table 2 [9,15–38] collects all the original experiment work on thermodynamic properties of Al–Cu system phase. The enthalpy of mixing of the liquid phase was firstly measured by Kawakami [15], which is accepted in [39]. Hultgren [16] published a set of data provided by Yasava and Itagaki as private communication, followed by their publication in [17]. Yasava's data [16,17] are much less exothermic than Kawakami's data [15,39]. The later published liquid enthalpy of mixing data [18–21,35] measured by high

Table 2
Summary of the experimental investigations for the Al–Cu binary system.

Quantity measured	Method	Temperature (°C)	Composition (at% Cu)	Refs.
$\Delta_m^{Liquid} H$	Calorimetry	1130	10–90	[15]
	Calorimetry	1100	10–90	[16]
	Adiabatic calorimetry	1100	11–92	[17]
		1084	4–44	[18] cited in [19]
	Calorimetry	1194	5.2–80.1	[19]
	Calorimetry	1177	9.8–39.9	[20]
	Drop calorimetry	700	0–40	[21]
$\Delta_f^{solid} H$	Calorimetry	20	15.7–92	[22]
	Calorimetry	325	50–66.7	[23]
	Calorimetry	30	63–86	[24]
	Calorimetry	500	0.4–98.4	[25]
a_{Al}^{liquid}, a_{Cu}^{liquid}	EMF	700, 800, 900	15.1–48.8	[26]
	EMF	1100	10–94.97	[27]
	Bubbling method	1100–1200	8.8–57.4	[28]
	EMF	1100	70–90	[29]
	Mass spectrometry	1100–1200	0–100	[30]
	Vapor pressure	1100	12–95	[31]
	Mass spectrometry	1000–1400	4.5–90.9	[32]
$\bar{H}_{Al}^{Liquid}$, $\bar{H}_{Cu}^{Liquid}$	Isothermal calorimeter	1200	0–60	[33]
	Solution calorimeter	918	00.14–1.96	[34]
	Isoperibolic calorimetry	1317	0–70	[35]
μ_{Al}^{Solid}	EMF	660–760	64.5–97.5	[36]
	EMF	400–550	40–62	[37]
	EMF	500	0.4–98.4	[25]
	EMF	777	65–96	[38]
Phase equilibria[a]	DTA, EDS, XRD	400–1050	10–83	[9]

[a] Only one detailed phase diagram study was found to be published after the basic assessment of the experimental phase diagram by MSIT [8].

temperature calorimeter were in agreement with [15,39] except the point at 60 at% Cu; they show no obvious temperature dependence from 700 °C to 1317 °C. Some partial enthalpy of mixing data of the liquid were measured by isothermal calorimetry [33,34]. All available activity data of Al in the liquid phase measured by electromotive force (EMF) and vapor pressure [26–32] are consistent with each other, except a few data points in [29,31] slightly deviate from the others. The enthalpy of formation of solid alloys was determined calorimetrically at room temperature [22–24] and at 500 °C [25] by using different calorimetric techniques. The chemical potential of Al in the solid phases was measured by EMF [25,36–38].

2.3. Phase equilibria

Murray [2] reviewed all experimental results prior to 1985 and plotted an evaluated Al–Cu phase diagram. Liu et al. [40] studied the Cu-rich Al–Cu phase equilibria and determined the γ_0/γ_1 transition as a second order transition, and discard the existence of a high temperature β_0 phase evaluated by [2]. Gröbner [8] updated the assessed experimental Al–Cu phase diagram which is mainly a combination of the review of [2] and the work of [40]. Ponweiser et al. [9] re-investigated the whole Al–Cu system, and mainly focused on the η_1 phase, and they also provided their evaluated experimental phase diagram. The solubility range of the some intermediate phases, η_1, η_2, ζ_1 and ζ_2, in [9] are contradicting [2,8], while the temperatures of the invariant reactions show better agreement [8,9]. The δ phase, also named as γ_2 phase in some publications, with orthorhombic *R3m* structure and often reported as R-type brass [41,42,43], was assessed with a solubility range of 59.3–61.9 at% Cu in [2,8]. However, the phase boundaries are not well determined in the original sources [13,42–44], and a single phase region covering both the δ and γ_1 phases is marked as questionable area in [9]. The coexistence of ζ_1 and γ_1 phase was also reported [45]. The two-phase region between γ_0-AlCu and γ_1-Al_4Cu_9 was assessed by dashed lines in [2]. Liu et al. [40] clarified the disorder–order transition between γ_0-AlCu and γ_1-Al_4Cu_9 phase. The thermal analysis results of [9] further confirmed that as disorder–order transition. In the present work, we essentially accept the assessed phase diagram data in [8] amended with the experimental data in [9].

3. Thermodynamic modeling

All equations for the Gibbs energy functions and the notation are the same as given in Part I of this work [46]. The Gibbs energies of the pure components are accepted from the SGTE compilation by Dinsdale in the most recent electronic version (SGTE-Unary-v5.1b, 24 November 2010, www.sgte.org), which is identical with the print version [47], except that more figures for the parameters of Al are given. The Gibbs energies for liquid, the terminal Fcc phase, denoted as (Al) and (Cu), and the intermediate phase Bcc, denoted as β and ε_1, are described by the substitutional solution model. The Gibbs energies of the two intermediate phases η_2 ($Al_{48}Cu_{52}$), δ_1 (Al_5Cu_8) and α_2 ($Al_{23}Cu_{77}$), assumed to be stoichiometric, are described by a Gibbs energy of formation term relative to pure Al and Cu (Fcc). The Gibbs energies of all other intermediate phases are described by the compound energy formalism (CEF) [48,49], allowing for a certain solution range.

Proper sublattices have been selected for the phases according to their crystal structure and composition range shown in Table 1. The θ phase is modeled as (Al)2(Al,Cu)1 and the η_1 phase as (Al)1 (Al,Cu)1, which are the same as in [4]. Only one η phase was considered in [4], and the calculated η phase region extends to low Cu side at low temperature. However, the experimental works [8,9] show that the low temperature η_2 phase contains higher Cu content than the high temperature η_1 phase. In this work, a stoichiometric phase η_2 was introduced with a model of (Al)48(Cu)52. As discussed in Section 2.3, the crystal structure and composition range of the δ_1 phase is still under dispute. In [2], the δ_1 phase was assessed as γ-brass structure together with the γ_0-AlCu, γ_1-Al_4Cu_9 phases, and with a composition range of 59.3–61.9% Cu. We modeled the δ_1 phase as stoichiometric (Al)5(Cu)8 phase for simplicity.

In the present work, the γ_0-AlCu phase is renamed as γ_2 phase in order to obtain a consistent notation in combination with the Cu–Zn binary system. To reflect the crystal structure of the disordered γ_2 phase in detail the four-sublattice model (**Al,Cu**)4(**Cu**)4 (**Cu**)6(**Al,Cu**)12 should be used. As the same simplification applied in the Cu–Zn binary system [46], we joined the first and forth sublattices to get the model (**Cu**)4(**Cu**)6(**Al,Cu**)16. For the ordered γ_1 phase, a six-sublattice model (Al,**Cu**)2(**Al**,Cu)2(**Cu**)4(**Cu**)6(**Al**,Cu) 6(Al,**Cu**)6 should be used to model the order/disorder transition; it is obtained by splitting the first and forth sublattices of the detailed model of γ_2, thus allowing the ordering. In this work, the γ_1/γ_2 transition is not modeled as order–disorder transition, but as first order transition; γ_1 and γ_2 are treated as two separate phases, and the model of the γ_1 phase is also simplified by combining all the sublattices containing both Al and Cu as (**Cu**)4(**Cu**)6(**Al,Cu**)16. This model partially reflects the crystal structure of the γ phase

and is just simplified sufficiently for a realistic joining with the γ-CuZn phase in the modeling of the Al–Cu–Zn ternary system, as discussed in [50].

Table 3
Phase names; name in tdb-parameters; models (sublattice formula), and parameters of the Gibbs energy equations developed in present work. Gibbs energy is given in J mol-formula^{-1} and temperature (T) is given in Kelvin. The Gibbs energies for the pure elements are found in the SGTE compilation [47].

Liquid; Liq; $(Al,Cu)_1$

$L^{0,Liq}_{Al,Cu} = -67094+8.555\times T$
$L^{1,Liq}_{Al,Cu} = 32148-7.118\times T$
$L^{2,Liq}_{Al,Cu} = 5915-5.889\times T$
$L^{3,Liq}_{Al,Cu} = -7290+5.5\times T$

(Al), (Cu); Fcc; $(Al,Cu)_1$
$L^{0,Fcc}_{Al,Cu} = -53520+2\times T$
$L^{1,Fcc}_{Al,Cu} = -39005-2.368\times T$
$L^{2,Fcc}_{Al,Cu} = 1210$

α_2; Alpha2; $(Al)_{0.23}(Cu)_{0.77}$
$G^{0,Alpha2}_{Al:Cu} = -13904.9-3\times T+0.23\times G^{0,Fcc}_{Al}+0.77\times G^{0,Fcc}_{Cu}$

β, ε_1; Bcc; $(Al,Cu)_1$
$L^{0,Bcc}_{Al,Cu} = -73537+3.98\times T$
$L^{1,Bcc}_{Al,Cu} = 51696-12\times T$

γ_1; Gam1; $(Cu)_4(Cu)_6(Al,Cu)_{16}$
$G^{0,Gam1}_{Cu:Cu:Al} = -94322.4+389.508\times T+16\times G^{0,Fcc}_{Al}+10\times G^{0,Fcc}_{Cu}$
$G^{0,Gam1}_{Cu:Cu:Cu} = -2600+26\times G^{0,Fcc}_{Cu}$
$L^{0,Gam1}_{Cu:Cu:Al,Cu} = -1613680-708\times T$
$L^{1,Gam1}_{Cu:Cu:Al,Cu} = -1585780-100\times T$

γ_2; Gam2; $(Cu)_4(Cu)_6(Al,Cu)_{16}$
$G^{0,Gam2}_{Cu:Cu:Al} = -94322.4+389.508\times T+16\times G^{0,Fcc}_{Al}+10\times G^{0,Fcc}_{Cu}$
$G^{0,Gam2}_{Cu:Cu:Cu} = 2600+26\times G^{0,Fcc}_{Cu}$
$L^{0,Gam2}_{Cu:Cu:Al,Cu} = -1451526.6-859.628\times T$
$L^{1,Gam2}_{Cu:Cu:Al,Cu} = -1516652.4-92\times T$

δ_1; Al5Cu8; $(Al)_5(Cu)_8$
$G^{0,Al5Cu8}_{Al:Cu} = -278450+5.2\times T+5\times G^{0,Fcc}_{Al}+8\times G^{0,Fcc}_{Cu}$

ζ; Al9Cu11; $(Al,Cu)_9(Cu)_{11}$
$G^{0,Al9Cu11}_{Al:Al} = 20\times G^{0,Bcc}_{Al}$
$G^{0,Al9Cu11}_{Al:Cu} = -424720+20\times T+9\times G^{0,Fcc}_{Al}+11\times G^{0,Fcc}_{Cu}$
$L^{0,Al9Cu11}_{Al,Cu:Cu} = 0$
$L^{1,Al9Cu11}_{Al,Cu:Cu} = -413300+100\times T$

ε_2; Eps2; $(Al,Cu)_1(Cu)_1$
$G^{0,Eps2}_{Al:Cu} = -40326+4.1\times T+G^{0,Fcc}_{Al}+G^{0,Fcc}_{Cu}$
$G^{0,Eps2}_{Cu:Cu} = 14850+30.1\times T+2\times G^{0,Fcc}_{Cu}$
$L^{0,Eps2}_{Al,Cu:Cu} = -56870-55\times T$

η_1; Eta1; $(Al,Cu)_1(Cu)_1$
$G^{0,Eta1}_{Al:Cu} = -39431+1.9\times T+G^{0,Fcc}_{Al}+G^{0,Fcc}_{Cu}$
$G^{0,Eta1}_{Cu:Cu} = 4770+9\times T+2\times G^{0,Fcc}_{Cu}$
$L^{0,Eta1}_{Al,Cu:Cu} = 0$
$L^{1,Eta1}_{Al,Cu:Cu} = -43168-18.5\times T$

η_2; Eta2; $(Al)_{0.48}(Cu)_{0.52}$
$G^{0,Eta2}_{Al:Cu} = -20987+1.62\times T+0.48\times G^{0,Fcc}_{Al}+0.52\times G^{0,Fcc}_{Cu}$

θ; Al2Cu; $(Al)_2(Al,Cu)_1$
$G^{0,Al2Cu}_{Al:Al} = 3\times G^{0,Bcc}_{Al}$
$G^{0,Al2Cu}_{Al:Cu} = -48361+8\times T+2\times G^{0,Fcc}_{Al}+G^{0,Fcc}_{Cu}$
$L^{0,Al2Cu}_{Al:Al,Cu} = 2211$

3.1. Parameter optimization

The thermodynamic parameters from [7] were used as a start point. Then the new models for the γ_1, γ_2, δ_1 and η_2 phases were introduced, finally α_2. At last, all the parameters of the phases were optimized based on all assessed experimental data. Many tries and iteration have been carried out during the optimization. Thermodynamic calculations and the parameter optimization are performed using the Pandat software package (www.computherm.com) with PanOptimizer [51]. All thermodynamic Gibbs energy parameters determined in the present work are given in Table 3.

4. Results and discussion

4.1. Phase diagram

Fig. 1 represents the calculated phase diagram of Al–Cu system in this work. This diagram is essential to clearly assign the current phase notation to all single phase regions of this complex system. Fig. 2 compares the calculated phase diagram with experimental data [8–11]. The plotted "experimental" phase diagram is taken from the most recent and comprehensive critical review performed by Gröbner [8], and the more recent experimental data points are shown in original from [9–11]. For better readability, "original" data points essentially found in [2] are not shown here, the reader is referred to the compilation in [8].

The calculated result shows good agreement with experimental phase diagram [8,9,11], especially for the important invariant reaction temperatures. In case of disagreement between the experimental assessment [8] and the more recent and meticulous experimental data of [9] the latter have been accepted for the present modeling, e.g. in the region of the γ_1/γ_2 transition, and the eutectoid $\beta \leftrightarrow \gamma_1+(Cu)$, etc. Table 4 shows the calculated invariant reactions compared with experimental data [2,8,9] and previous Calphad calculations [4,5,7]. Murray [2] provided an assessed phase diagram enlarged at Al-rich corner compared with all original experimental data. The calculated results, especially the solvus line of (Al), agree well with the experimental phase diagram [2] as shown in Fig. 3.

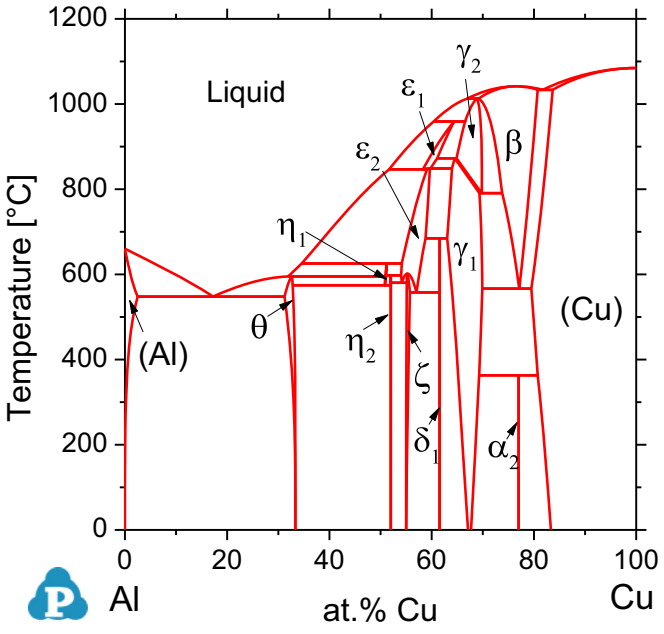

Fig. 1. Calculated phase diagram of the Al–Cu system from the present thermodynamic description.

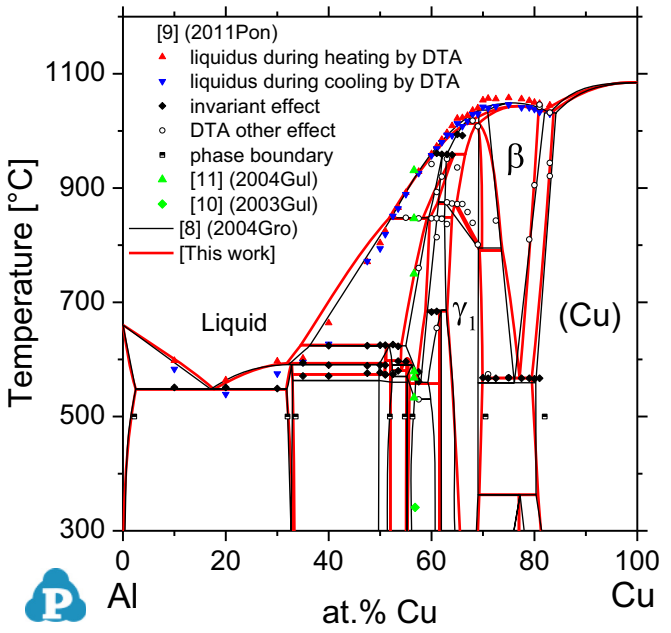

Fig. 2. Comparison of the Al–Cu phase diagram calculated in this work with the assessed experimental phase diagram by MSIT [8] and more recent experimental data [9–11]. Additional short-hand notation indicating year and first author is given.

The DTA results in [9] and the assessed experimental phase diagrams [2,8] show the existence of the η_1/η_2 phase transition within the η phase. It is most clearly seen in the almost degenerate reaction $\eta_1 \leftrightarrow \eta_2+\theta$ measured at 574 °C [9], 11 K above the 563 °C in the previous assessments [2, 8]. Due to the solution range in the η_1/η_2 phases the second invariant temperature related to the η_1/η_2 transition, $\eta_1+\zeta_{(2)} \leftrightarrow \eta_2$, is measured at higher temperature, 580 °C, by a single sample [9]. We acknowledge the transition and treat η_1 and η_2 as separate phases, as opposed to all previous Calphad assessments treating it as one η phase [4,7]. However, due to the scarcity of data, the η_2 phase is modeled as stoichiometric phase of $Al_{48}Cu_{52}$. The temperature of the reaction $\eta_1 \leftrightarrow \eta_2+\theta$ is calculated at 573.7 °C, close to the experimental result of 574 °C [9]. In addition, two other invariant reactions associate with η_2 phase are calculated, $\varepsilon_2+\eta_1 \leftrightarrow \eta_2$ (597.9 °C) and $\varepsilon_2 \leftrightarrow \eta_2+\zeta$ (580.4 °C). These temperatures are very close to detected thermal events at 597 °C and 580 °C corresponding to invariant reactions [9], but were attributed to different reactions associated with the ζ_2 phase [9]. The $\zeta_2(\zeta_1)$ phase is not well studied and assumed (or speculated) to possess a large solubility range as discussed below.

Gulay and Harbrecht [10, 11] clearly determined the crystal structures of ζ_1 (oF88, *Fmm2*) and ζ_2 (oI24, *Imm2*) phases and also carried out DSC measurements. The calculated results in this work agree well with five of the detected thermal signals of alloy Al43.4Cu56.6 (ζ_1-Al_3Cu_4) at heating in the range 568–931 °C [11], see Fig. 2. The origin of the signal at 533 °C in that sample remains unclear because the previously assumed ζ_1/ζ_2 transition near that temperature [2,8,9] is highly questionable based on the results of [10,11] as discussed below.

Gulay et al. [11] also found that the ζ_1-phase resists a heat treatment at 400 °C for 10 days, which questions the currently assumed decomposition of this high-temperature phase ζ_1 at 530 °C based on thermal signals [8,2]. In their second work, Gulay et al. [10] showed that the ζ_2–$Al_3Cu_{4-\delta}$ phase, currently perceived as stable low-temperature phase [2,8], decomposes during heat treatment at 400 °C into ζ_1 (plus some η_2). Thus, ζ_1 even forms at 400 °C, which puts a further question mark on the previously assumed thermal stability ranges [2,8] of the "ζ" phases. They also

Table 4
Comparison of calculated and experimental invariant reactions in the Al–Cu system.

Reaction	T/°C	Cu content in phases at%			Reference/ comments
Congruent		L	β		
L↔β	1049	75	75		[2,8]
	1052 ± 5				[9] Exp.
	1045.6	76.6	76.6		[4] Calphad
	1045.6	76.6	76.6		[5] Calphad
	1043.9	76.8	76.8		[7] Calphad
	1043.3	**76.7**	**76.7**		**[This work]**
Eutectic		L	(Cu)	β	
L↔(Cu)+β	1032	83.0	84.2	82.0	[2,8]
	1035 ± 5	83.0 ± 0.5	84.5 ± 0.5	82.0 ± 0.5	[9] Exp.
	1036.1	81.8	83.7	80.7	[4] Calphad
	1036.1	81.7	83.7	80.7	[5] Calphad
	1036.1	81.7	83.7	80.7	[7] Calphad
	1035.1	**81.8**	**83.7**	**80.8**	**[This work]**
Peritectic		L	β	γ_2	
L+β↔γ_2	1037	69.2	70.9	~ 69	[8]
	993 ± 2	63.0 ± 0.5	69.0 ± 0.5	65.0 ± 1.0	[9] Exp.
	1020.3	67.9	69.9	68.4	[4] Calphad
	1019.0	67.9	69.9	68.4	[5] Calphad
	1019.0	67.9	69.9	68.4	[7] Calphad
	1013.2	**66.9**	**69.2**	**68.8**	**[This work]**
Peritectic		γ_2	L	ε_1	
γ_2+L↔ε_1	958	62.9	59.8	62.1	[2,8]
	960 ± 2	65.5 ± 0.5	60.0 ± 0.5	64.5 ± 0.5	[9] Exp.
	959.2	66.7	60.4	64.4	[4] Calphad
	959.1	66.7	60.4	64.4	[5] Calphad
	959.1	66.7	60.4	64.4	[7] Calphad
	959.3	**66.5**	**60.4**	**64.4**	**[This work]**
Peritectoid		ε_1	γ_2	γ_1	
$\varepsilon_1+\gamma_2 \leftrightarrow \gamma_1$	873	61.4	66.0	63.9	[2]
($\gamma_2 \leftrightarrow \gamma_1$, ε_1)	874 ± 2		65.0		[9] Exp.
$\varepsilon_1+\gamma_2 \leftrightarrow \gamma_1$	877.4	62.5	65.6	64.7	[4] Calphad
$\varepsilon_1+\gamma_2 \leftrightarrow \gamma_1$	880.7	62.6	65.6	64.8	[5] Calphad
$\varepsilon_1+\gamma_2 \leftrightarrow \gamma_1$	876.7	62.5	65.6	64.7	[7] Calphad
$\varepsilon_1+\gamma_2 \leftrightarrow \gamma_1$	**872.5**	**61.1**	**64.9**	**64.5**	**[This work]**
Deg., Ptd.,Cat. [a]		ε_1	ε_2	L	
$\varepsilon_1 \leftrightarrow \varepsilon_2$, L	848	~59.4	~59.4	52.2	[2,8]
$\varepsilon_1 \leftrightarrow \varepsilon_2$, L	847 ± 1	59.5 ± 0.5	59.5 ± 0.5	52.5 ± 0.5	[9] Exp.
ε_1+L↔ ε_2	850.1	58.5	57.7	52.0	[4] Calphad
ε_1+L↔ ε_2	851.1	58.5	57.7	52.0	[5] Calphad
ε_1+L↔ ε_2	851.1	58.5	57.7	52.0	[7] Calphad
$\varepsilon_1 \leftrightarrow \varepsilon_2$+L	**846.6**	**58.3**	**59.1**	**51.7**	**[This work]**
Ptd., Deg., Etd.[a]		γ_1	ε_1	ε_2	
$\gamma_1+\varepsilon_1 \leftrightarrow \varepsilon_2$	850	62.5	~61.1	~61.1	[2,8]
$\varepsilon_1 \leftrightarrow \varepsilon_2$, γ_1	847 ± 1	64.0 ± 0.5	62.5 ± 0.5	62.5 ± 0.5	[9] Exp.
$\varepsilon_1 \leftrightarrow \varepsilon_2+\gamma_1$	836.2	63.6	60.2	58.1	[4] Calphad
$\varepsilon_1 \leftrightarrow \varepsilon_2+\gamma_1$	837.0	63.9	60.2	58.0	[5] Calphad
$\varepsilon_1 \leftrightarrow \varepsilon_2+\gamma_1$	836.4	63.5	60.2	58.0	[7] Calphad
$\varepsilon_1 \leftrightarrow \varepsilon_2+\gamma_1$	**848.7**	**64.0**	**59.8**	**59.7**	**[This work]**
Deg., Etd.[a]		γ_2	β	γ_1	
($\gamma_2 \leftrightarrow \gamma_1$, β)	~ 800	69.0			[9] Exp.
$\gamma_2 \leftrightarrow \beta+\gamma_1$	781.1	68.9	73.2	68.7	[4] Calphad
$\gamma_2 \leftrightarrow \beta+\gamma_1$	781.3	69.0	73.2	68.9	[5] Calphad
$\gamma_2 \leftrightarrow \beta+\gamma_1$	781.1	68.9	73.2	68.7	[7] Calphad
$\gamma_2 \leftrightarrow \beta+\gamma_1$	**790.7**	**69.8**	**73.8**	**69.3**	**[This work]**
Peritectoid		γ_1	ε_2	δ_1	
$\gamma_1+\varepsilon_2 \leftrightarrow \delta_1$	686	62.8	59.2	61.9	[2,8]
	684 ± 1	63.0 ± 0.5	58.5 ± 0.5	61.5 ± 0.5	[9] Exp.
	686.6	62.8	57.2	60	[4] Calphad
	690.2	63.7	57.2	60	[5] Calphad
	686.6	62.8	57.2	60	[7] Calphad
	684.6	**63.0**	**58.8**	**61.5**	**[This work]**
Peritectic		ε_2	L	η_1	
ε_2+L↔η_1	624	55.0	36.3	51.8	[2,8]
	625 ± 2	54.5 ± 0.5	38.5 ± 0.5	52.0 ± 0.5	[9] Exp.
	624.9	54.1	34.6	51.0	[4] Calphad
	625.0	54.1	34.9	51.0	[5] Calphad
	625.0	54.1	34.9	51.0	[7] Calphad
	625.0	**54.1**	**34.6**	**51.2**	**[This work]**
Peritectic		η_1	L	θ	
η_1+L↔θ	591	49.8	32.2	32.8	[2,8]
	591 ± 2	51.5 ± 0.5	32.5 ± 0.5	33.5 ± 0.5	[9] Exp.
	595.9	50.6	31.9	32.9	[4] Calphad

Table 4 (*continued*)

Reaction	T/°C	Cu content in phases at%			Reference/ comments
	595.7	50.6	32.2	32.9	[5] Calphad
	595.7	50.6	32.2	32.9	[7] Calphad
	593.3	**50.9**	**31.9**	**32.9**	**[This work]**
Etd., Ptd. [a]		ε_2	η_1	ζ	
$\varepsilon_2+\eta_1 \leftrightarrow \zeta_1$	590	56.5	52.4	56.2	[2,8]
$\varepsilon_2+\eta_1 \leftrightarrow \zeta_2$	597 ± 1	56.5 ± 0.5	53.0 ± 0.5	55.5 ± 0.5	[9] Exp.
$\varepsilon_2 \leftrightarrow \eta+\zeta$	579.3	54.3	51.1	55	[4] Calphad
$\varepsilon_2 \leftrightarrow \eta+\zeta$	579.3	54.3	51.1	55	[5] Calphad
$\varepsilon_2 \leftrightarrow \eta+\zeta$	579.3	54.3	51.1	55	[7] Calphad
		ε_2	η_1	η_2	
$\varepsilon_2+\eta_1 \leftrightarrow \eta_2$	**597.9**	**54.0**	**51.2**	**52**	**[This work]**
Ptd., Etd. [a]		η_1	ζ	η_2	
$\eta_1 \leftrightarrow \eta_2+\zeta_2$	560	~52.3	55.3	~52.3	[2,8]
$\zeta_1+\eta_1 \leftrightarrow \zeta_2$	570	52.3	55.2		[2,8]
$\eta_1+\zeta_2 \leftrightarrow \eta_2$	580 ± 1	52.5 ± 0.5	54.5 ± 0.5	52.5 ± 0.5	[9] Exp.
Eutectoid		ε_2	ζ	η_2	
$\varepsilon_2 \leftrightarrow \eta_2+\zeta$	**580.4**	**54.1**	**55.1**	**52**	**[This work]**
Eutectoid		η_1	θ	η_2	
$\eta_1 \leftrightarrow \theta+\eta_2$	563	49.8	33.0	49.8	[2,8]
	574 ± 3	52.0 ± 0.5	33.5 ± 0.5	52.5 ± 0.5	[9] Exp.
	573.7	**50.9**	**32.9**	**52**	**[This work]**
Eutectoid		β	(Cu)	γ_1	
$\beta \leftrightarrow$(Cu)$+\gamma_1$	567	76.1	80.3	69.0	[2]
	559	76.1	80.3	69.0	[8]
	567 ± 2	76.0 ± 0.5	81.5 ± 0.5	70.0 ± 0.5	[9] Exp.
	564.7	77.1	79.5	69.1	[4] Calphad
	566.9	77.1	79.5	70.5	[5] Calphad
	564.7	77.1	79.5	69.1	[7] Calphad
	567.5	**77.1**	**79.5**	**69.9**	**[This work]**
Eutectoid		ε_2	ζ	δ_1	
$\varepsilon_2 \leftrightarrow \zeta+\delta_1$	560	57.9	56.9	59.3	[2,8]
	582.7	55.6	55	60	[4] Calphad
	582.7	55.6	55	60	[5] Calphad
	582.7	55.6	55	60	[7] Calphad
	557.7	**57.0**	**55.7**	**61.5**	**[This work]**
Eutectic		L	θ	(Al)	
L$\leftrightarrow\theta+$(Al)	548.2	17.1	31.9	2.48	[2,8]
	550 ± 2	17.0 ± 1.0	32.0 ± 0.5	2.5 ± 0.5	[9] Exp.
	547.6	17.5	31.8	2.54	[4] Calphad
	547.5	17.5	31.8	2.54	[5] Calphad
	547.5	17.5	31.8	2.54	[7] Calphad
	547.7	**17.7**	**31.8**	**2.50**	**[This work]**
Peritectiod		γ_1	(Cu)	α_2	
γ_1+(Cu)$\leftrightarrow\alpha_2$	363	69	80.3	77.25	[2,8]
	363.0	**69.3**	**80.7**	**77**	**[This work]**

[a] The type of these reactions differ in different references. Abbreviations used here are Ptd.: Peritectoid; Deg.: Degenerate; Cat.: Catatectic; Etd.: Eutectoid.

detected a small but reproducible exothermic effect on cooling single-phase ζ_2 in DSC at 341 °C [10], (see Fig. 2). That might be a kinetic effect of ζ_2-sample transition/decomposition considering the metastability of ζ_2 observed in the same work at 400 °C.

The ζ_1 and ζ_2 phases had previously been simplified to a single stoichiometric Al_9Cu_{11} phase [4,7]. However, solution ranges exist even though not very well established. The ζ_1/ζ_2 transition and thermal stability ranges are highly questionable [10,11]. Therefore, it is modeled in the present work as a single phase, ζ, with a narrow solution range close to the Al_9Cu_{11} composition.

The phase labeled δ_1 is modeled in the present work as stoichiometric Al_5Cu_8, which is closer to the experimentally determined composition, see Fig. 2, as compared to the previously assumed model, Al_2Cu_3 [4,7], see Fig. 4. The simplification as stoichiometric phase is considered reasonable because the solution range of that phase is not well established [9].

The γ_1/γ_2 transition modeled as very narrow two-phase region, is very close to the experimentally determined order–disorder transition line [9]. Also the eutectoid $\beta=\gamma_1+$(Cu) invariant

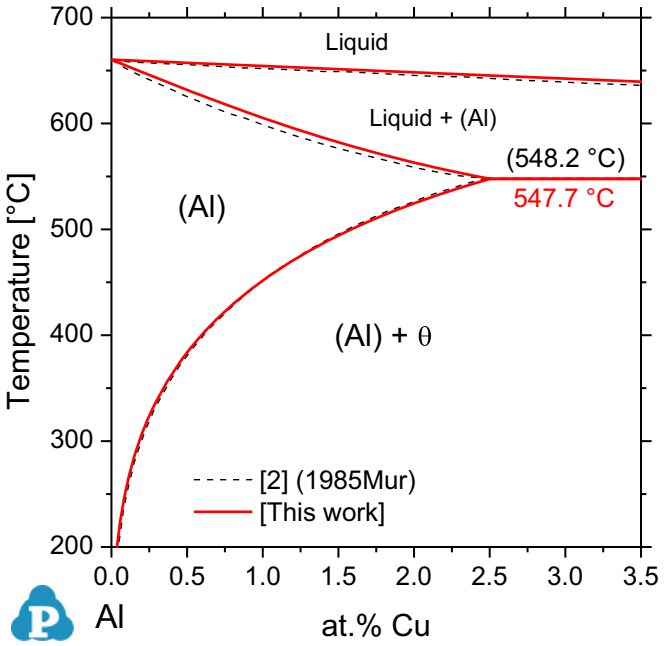

Fig. 3. Comparison of the Al–Cu phase diagram at Al-rich corner calculated in this work with the assessed experimental phase diagram [2].

temperature is in excellent agreement with the experimental data [9], see Fig. 2. Moreover, the single-phase ε_2 phase region in this work agrees better with the experimental phase diagram [2,8] than previous calculations [4,7].

The calculated liquidus line of β is slightly below the experimental data, whereas the liquidus of ε_2 is slightly above, see Fig. 2. It is hard to reduce this deviation while maintaining the very good agreement with the invariant reaction temperatures, see Table 4, and all other thermodynamic and phase equilibrium data. The same deviation is observed in previous Calphad calculations [4,7], as shown in Fig. 4. However, a slight improvement is obtained in the present work, especially for the ε_2 liquidus.

It is noted that the calculated phase diagrams of [4] and [7] virtually overlap, the only visible distinction in Fig. 4 is the $(\delta_1+\gamma_1)/\gamma_1$ phase boundary, which veers off to much lower Cu content with decreasing temperature in the diagram of Saunders [4]. That produces a very unrealistic shape of the $(\delta_1+\gamma_1)/\gamma_1$ phase boundary at low temperature and an artificial eutectoid $(\delta_1=\zeta+\gamma_1)$ at −60.4 °C. In addition, one of the liquid phase parameters was selected in a way making the enthalpy of mixing temperature dependent [4], a dependency that is not supported by any experimental data. Witusiewicz et al. [7] remediated both artifacts by revising the parameters of the liquid and the γ_1 phase, keeping all other parameters from [4]. However, all invariant reaction temperatures of these two calculations [4,7] generally agree within 1 K, the largest difference is 1.3 K at the peritectic $L+\beta=\gamma_2$ in Table 4, calculated at 1013.2 °C in the present work. One should also notice that the temperature of the invariant reaction of $L+\beta\leftrightarrow\gamma_2$ is determined to be 1037 °C in [8], but 933 ± 2 °C in [9], the present work and previous calculations cannot come close to either of them, thus an intermediate temperature between the reported values is accepted.

4.2. Thermodynamic properties of the liquid phase

Fig. 5 shows the reported experimental data [15–21,35] for the enthalpy of mixing of the liquid phase. Disregarding the data from [16,17], all other experimental data are agree well with each other,

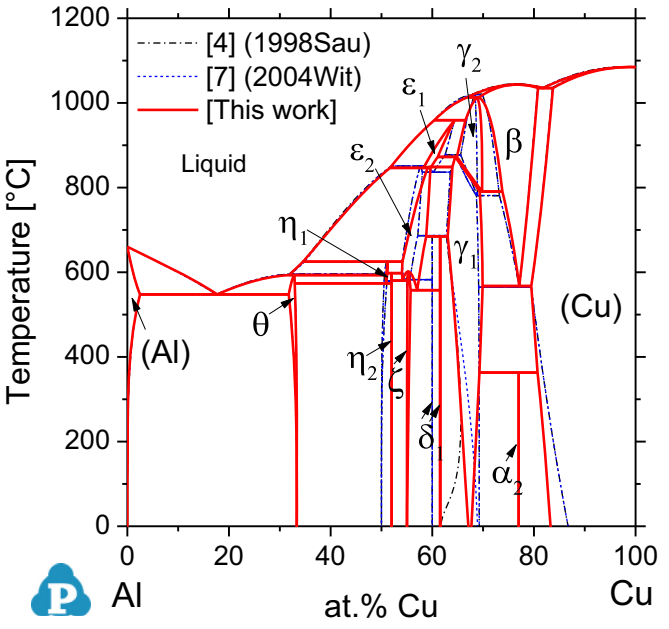

Fig. 4. Comparison of the calculated phase diagrams of the Al–Cu system in this work with previously published Calphad assessments [4,7].

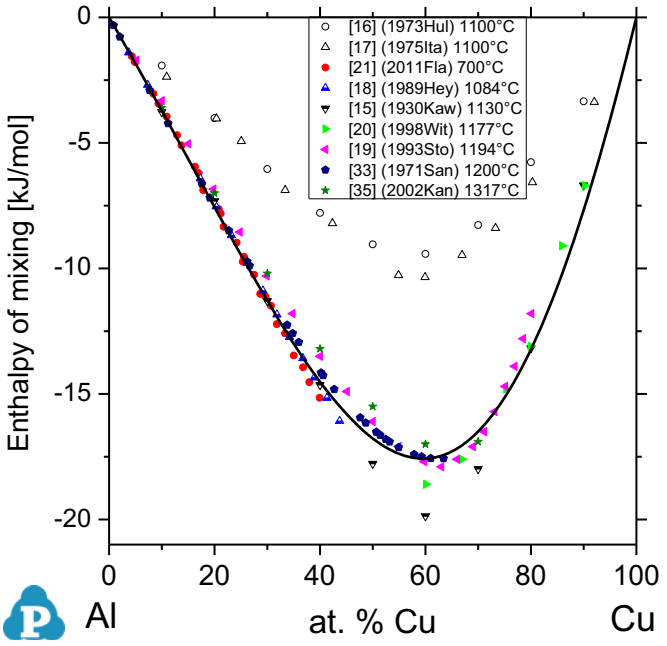

Fig. 5. Calculated enthalpy of mixing of the liquid phase compared with experimental data [16–21,33,35]. Reference states: pure liquid elements.

and do not show any temperature dependence from 700 °C to 1317 °C. Thus the implicit temperature dependence in the modeling of [4], who did not show any experimental data for comparison at all, is not justified. Actually, the data in [16] were provided as private communication by Yazawa and Itagaki, who are the authors of [17]. Those data are much more positive than the later determined enthalpy of mixing data [18–21,35], and thus not accepted in this work. The calculated partial enthalpies of the components in the liquid phase are also in good agreement with the experimental data as shown in Fig. 6.

Fig. 7 represents the calculated activity of the components in liquid at 1100 °C in agreement with experimental data from [26–32]. For better resolution of the aluminum activity, a_{Al}, in the Cu-rich region Fig. 8 shows these data as relative chemical potential, μ_{Al}-$G_{Al}^{0,Liquid} = RT \ln a_{Al}$. It reveals that the relative chemical potential data from [29,31], thus also a_{Al}, are slightly above the other experimental results [27,30,32], which are in perfect agreement with the calculated curve.

4.3. Thermodynamic properties of solid phases

Fig. 9 represents the calculated enthalpy of formation of the solid phases at 500 °C compared with the experimental data and a calculation using the parameters of [7]. Fig. 10 shows the relative chemical potential of Al in the solid phases, the calculated results from this work are compared with experimental data and a calculation using the parameters of [7]. Some deviations are noted and we found that it is difficult to obtain a closer agreement with the experimental data in Fig. 9 and Fig. 10 while maintaining the good agreement with the phase diagram and liquid phase thermodynamic data. The largest deviation is between 63–69 at% Cu, corresponding to the $\delta_1+\gamma_1$ and the γ_1 phase regions, in which the phase boundary is still questionable as mentioned in [9]. Although different models have been applied for δ_1 and γ_1 phases in this work compared to previous Calphad modeling [7], similar deviations between calculated and experimental data are observed.

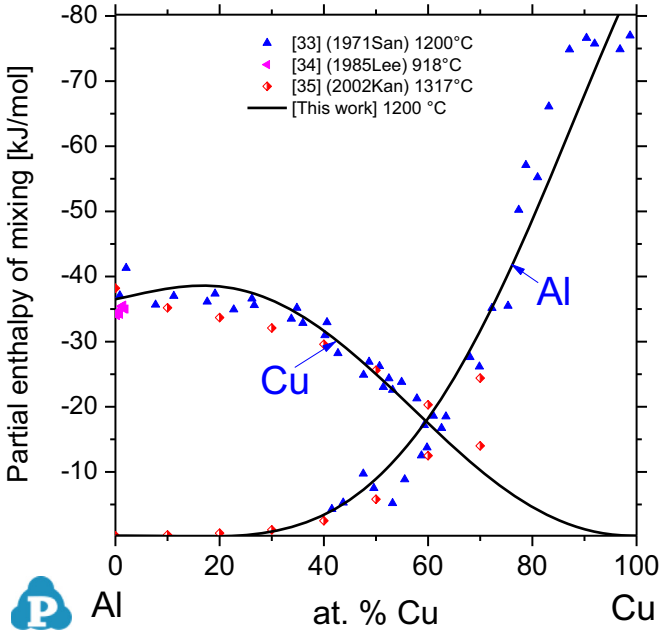

Fig. 6. Calculated partial enthalpy of the elements in the liquid phase (at 1200 °C) compared with experimental data [33–35]. Reference states: pure liquid elements.

5. Conclusion

The key improvements of this thermodynamic re-assessment compared to previous Calphad descriptions are:

- For the first time all available experimental data of the Al–Cu system have been extensively compared with calculated results.
- The model selected for the γ_1 and γ_2 phases partially reflects the crystal structure of the γ phase while being sufficiently simple for a realistic joining with the γ-CuZn phase in the Al–Cu–Zn ternary system.
- The γ_1/γ_2 transition, modeled as very narrow two-phase region, is very close to the experimentally determined order–disorder

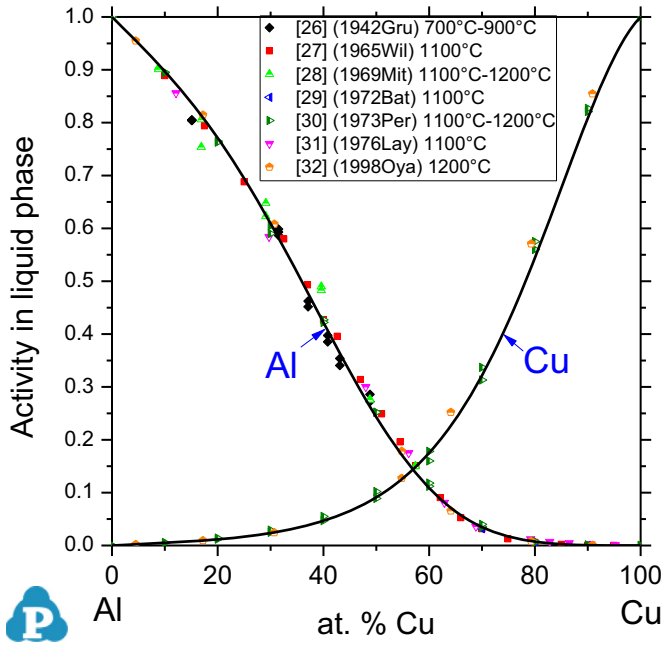

Fig. 7. Calculated activity of the elements in the liquid phase (at 1100 °C) agree well with the experimental data [26–32]. Reference states: pure liquid elements.

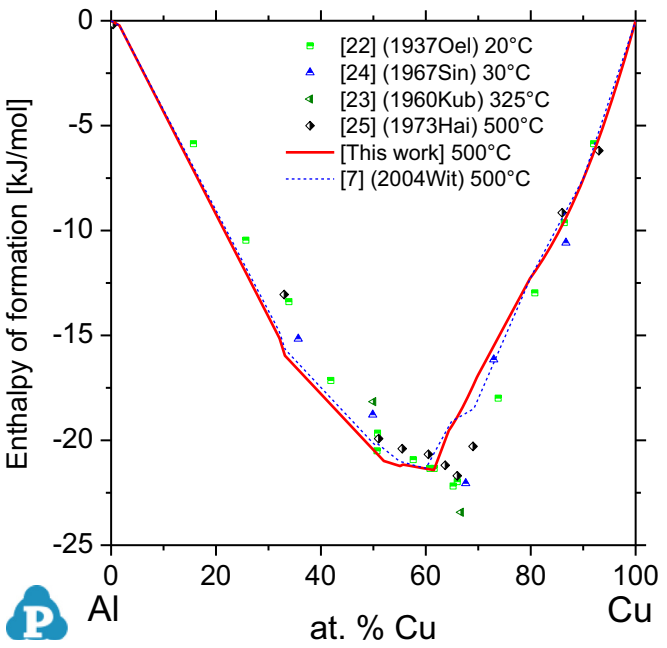

Fig. 9. Calculated enthalpy of formation of the solid phases (at 500 °C) from this work and [7] compared with experimental data [22–25] Reference states: solid Al (Fcc) and Cu (Fcc).

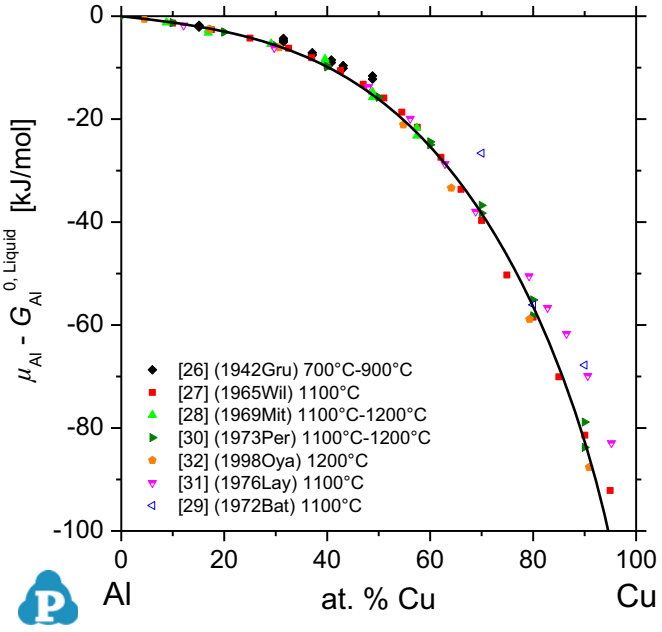

Fig. 8. Calculated relative chemical potential of Al (at 1100 °C) in the liquid phase compared with experimental data [26–32]. Reference state: liquid Al.

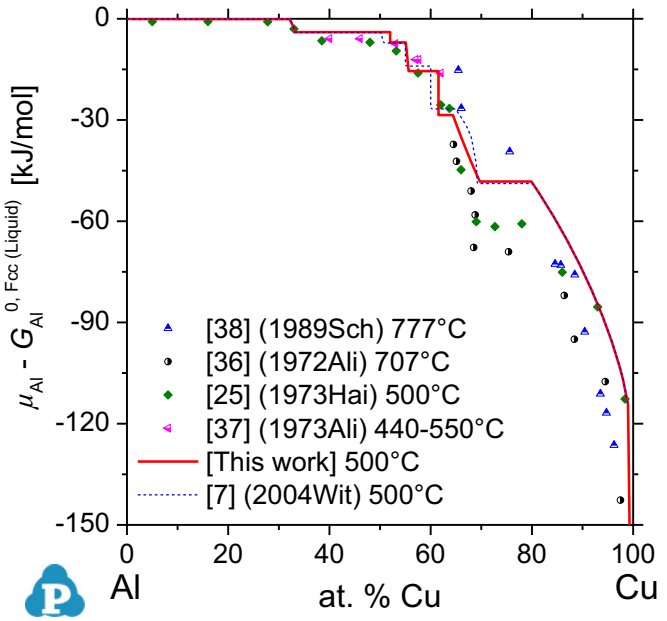

Fig. 10. Comparison of the relative chemical potential of Al in the solid phases obtained by experiments [25,36–38] and calculated using the present thermodynamic description. Reference state changes from solid Al (Fcc) at 500 °C to liquid Al for the experimental data at 707 °C and 777 °C.

transition line [9].

- The η_1/η_2 phase transition has been introduced, and the temperature of the invariant reactions associated with those two phases agree well with experimental thermal signals.
- The extent of single-phase ε_2 phase in this work agrees better with experimental data.
- The stoichiometry Al_5Cu_8 for the δ_1 phase is closer to the experimentally determined composition.
- The α_2 phase forming below 363 °C has been introduced.
- Very good agreement with the extensive thermodynamic properties of the liquid Al–Cu phase and reasonable agreement for solid phase thermodynamic properties is demonstrated in detail.

Acknowledgment

This study is supported by the German Research Foundation (DFG) under Grant no. Schm 588/41.

Appendix A. Supplementary material

Supplementary data associated with this article can be found in the online version at http://dx.doi.org/10.1016/j.calphad.2015.10.004.

References

[1] L. Kaufman, H. Nesor, Coupled phase diagrams and thermochemical data for transition metal binary systems-V, Calphad 2 (1978) 325–348.
[2] J.L. Murray, The aluminium–copper system, Int. Met. Rev. 30 (1985) 211–234.
[3] S.-W. Chen, Y.-Y. Chuang, Y. Austin Chang, M. Chu, Calculation of phase diagrams and solidification paths of Al-rich Al – Li – Cu alloys, Met. Trans. A 22 (1991) 2837–2848.
[4] N. Saunders, System Al-Cu, COST 507: thermochemical database for light metal alloys Volume 2: Definition of thermodynamical and thermophysical properties to provide a database for the development of new light alloys, in: I. Ansara, A.T. Dinsdale, M.H. Rand (Eds.), European Commission, 1998, pp. 28–33.
[5] H. Liang, Y.A. Chang, A thermodynamic description for the Al–Cu–Zn system, J. Phase Equilib. 19 (1998) 25–37.
[6] J. Miettinen, Thermodynamic description of the Cu–Al–Zn and Cu–Sn–Zn systems in the copper-rich corner, Calphad 26 (2002) 119–139.
[7] V.T. Witusiewicz, U. Hecht, S.G. Fries, S. Rex, The Ag–Al–Cu system: Part I: reassessment of the constituent binaries on the basis of new experimental data, J. Alloy. Compd. 385 (2004) 133–143.
[8] J. Gröbner, Al–Cu binary phase diagram evaluation, in: G. Effenberg (Ed.), Binary Evaluations, MSI, Materials Science International Services GmbH, Stuttgart, 2004.
[9] N. Ponweiser, C.L. Lengauer, K.W. Richter, Re-investigation of phase equilibria in the system Al-Cu and structural analysis of the high-temperature phase η_1-$Al_{1-\delta}Cu$, Intermetallics 19 (2011) 1737–1746.
[10] L.D. Gulay, B. Harbrecht, The crystal structure of ζ_2-$Al_3Cu_{4-\delta}$, Z. Anorg. Allg. Chem. 629 (2003) 463–466.
[11] L.D. Gulay, B. Harbrecht, The crystal structure of ζ_1-Al_3Cu_4, J. Alloy. Compd. 367 (2004) 103–108.
[12] G.D. Preston, XCIV. An X-ray Investigation of Some Copper–Aluminium, Alloys, Edinburgh, and Dublin Philosophical Magazine and Journal of Science, The London (1931), p. 980–993.
[13] A.J. Bradley, H. Lipson, An X-ray investigation of slowly cooled copper–nickel–aluminium alloys, Proc. R. Soc. Lond. A 167 (1938) 421–438.
[14] L.D. Gulay, B. Harbrecht, The crystal structures of the ζ_1 and ζ_2 phases in the Al–Cu system, Z. Anorg. Allg. Chem. 628 (2002) 2170-2170.
[15] M. Kawakami, A further investigation of the heat of mixture in molten metals, Sci. Rep. Tohoku Imp. Univ. Ser. 1 (19) (1930) 521–549.
[16] R. Hultgren, P.D. Desai, D.T. Hawkins, M. Gleiser, K.K. Kelley, Selected Values of the Thermodynamic Properties of Binary Alloys, American Society for Metals, Metals Park, Ohio, 1973.
[17] K. Itagaki, A. Yazawa, Heats of mixing in liquid copper or gold binary alloys, Trans. Jpn. Inst. Met. 16 (1975) 679–686.
[18] E. Heyer, University of Vienna, private communication to [19], 1989.
[19] U.K. Stolz, I. Arpshofen, F. Sommer, B. Predel, Determination of the enthalpy of mixing of liquid alloys using a high-temperature mixing calorimeter, J. Phase Equilib. 14 (1993) 473–478.
[20] V. Witusiewicz, U.K. Stolz, I. Arpshofen, F. Sommer, Thermodynamics of liquid Al–Cu–Zr alloys, Z. Met. 89 (1998) 704–713.
[21] H. Flandorfer, M. Rechchach, A. Elmahfoudi, L. Bencze, A. Popovič, H. Ipser, Enthalpies of mixing of liquid systems for lead free soldering: Al–Cu–Sn system, J. Chem. Thermodyn. 43 (2011) 1612–1622.
[22] W. Oelsen, W. Middel, Zur Thermochemie, I. der Legierungen, Unmittelbare Bestimmung der Bildungswaermen der Legierungsreihen Kobalt–Silizium, Eisen–Aluminium, Kobalt–Aluminium, Nickel–Aluminium, Kupfer–Aluminium und Antimon–Zink fuer den Gusszustand, Mitt. K. W. I für Eisenforsch. 19 (1937) 1–26.
[23] O. Kubaschewski, G. Heymer, Heats of formation of transition-metal aluminides, Trans. Faraday Soc. 56 (1960) 473–478.
[24] R.C. Sinvhal, P.R. Khangaonkar, Heats of formation of some aluminum alloys by differential calorimetry, Trans. Indian Inst. Met. 20 (1967) 107–110.
[25] J. Hair, D.B. Downie, Thermodynamic properties of the Cu–Al system: correlation with bonding mechanisms, Faraday Symp. Chem. Soc. 8 (1973) 56–63.
[26] G. Grube, P. Hantelmann, Polarisationsmessungen bei der elektrolytischen Raffination des Aluminiums nach dem Dreischichtenverfahren, I. Mitteilung, Z. Elektrochem. 48 (1942) 399–409.
[27] T.C. Wilder, The thermodynamic properties of the liquid aluminum–copper system, Trans. Met. Soc. AIME 233 (1965) 1202–1208.
[28] H. Mitani, H. Nagai, Determination of the activities of aluminum and cupper in liquid Al-Cu binary alloys by the bubbling method, J. Jpn. Inst. Met. 33 (1969) 344–348.
[29] G.I. Batalin, E.A. Beloborodova, V.N. Vasil'ev, Thermodynamic properties of molten alloys of aluminum with copper, Ukr. Khim. Zh. (Russ. Ed.) 38 (1972) 920–923.
[30] J. Perakis, C. Chatillon, A. Pattoret, High-temperature mass spectrometry. Thermodynamic properties of aluminum–copper liquid alloys, C. R. Acad. Sci., Ser. C 276 (1973) 1513–1516.
[31] D.I. Layner, L.M. Ostrovskaya, O.S. Serebryannikova, Activities of components in liquid Cu–Al alloys, Izv. Akad. Nauk. SSSR. Met. 15 (1976) 15–18.
[32] H. Oyamada, T. Nagasaka, M. Hino, Activity measurement of the constituents in liquid Cu–Al alloy with mass-spectrometry, Mater. Trans. JIM 39 (1998) 1225–1229.
[33] V.M. Sandakov, Y.O. Esin, P.V. Geld, V.D. Shantarin, Heats of formation of liquid copper–aluminium alloys, Russ. J. Phys. Chem. 45 (1971) 1150–1152.
[34] J.J. Lee, F. Sommer, The determination of the partial enthalpies of mixing of aluminium-rich alloy melts by solution calorimetry, Z. Met. 76 (1985) 750–754.
[35] D. Kanibolotsky, O. Bieloborodova, N. Kotova, V. Lisnyak, Thermodynamic properties of liquid Al–Si and Al–Cu alloys, J. Therm. Anal. Calorim. 70 (2002) 975–983.
[36] S.A. Ali, V.V. Samokhval, V.A. Geiderikh, A.A. Vecher, Thermodynamic properties of solid alloys of copper with aluminum, Russ. J. Phys. Chem. 46 (1972) 139–140.
[37] S.A. Ali, V.A. Geiderikh, Thermodynamic properties of copper–aluminum alloys, Russ. J. Phys. Chem. 47 (1973) 22–25.
[38] H.J. Schaller, G. Fickel, A. Maaz, Thermodynamic properties of solid copper–aluminum and copper–germanium alloys, NATO ASI Ser. C 286 (1989) 359–370.
[39] O. Kubaschewski, J.A. Catterall, Thermochemical Data of Alloys, Pergamon Press, London & New York, 1956.
[40] X.J. Liu, I. Ohnuma, R. Kainuma, K. Ishida, Phase equilibria in the Cu-rich portion of the Cu–Al binary system, J. Alloy. Compd. 264 (1998) 201–208.
[41] S. Westman, Phase Analysis at 660 °C of gamma region of copper–aluminium system, Acta Chem. Scand. 19 (1965) 2369–2372.
[42] Y. Funamizu, K. Watanabe, Interdiffusion in the Al–Cu system, Trans. Jpn. Inst. Met. 12 (1971) 147–152.
[43] M. Van Sande, J. Van Landuyt, M. Avalos-Borja, G.T. Villaseñor, S. Amelinckx, A reinvestigation of the γ phase in Cu–Al alloys: a new long-period superstructure, Mater. Sci. Eng. 46 (1980) 167–173.
[44] A.J. Bradley, P. Jones, An X-ray investigation of the copper-aluminum alloys, J. Inst. Met. 51 (1933) 131–157.
[45] X.L. Ma, A. Rüdiger, H. Liebertz, U. Köster, W. Liu, A new structural variant of ζ-Al_3Cu_4 and its orientation relationship with the cubic γ-Al_4Cu_9, Scr. Mater. 39 (1998) 707–714.
[46] Thermodynamic assessment of the Al–Cu–Zn system, part I: Cu–Zn binary system. Calphad http://dx.doi.org/10.1016/j.calphad.2015.09.010 50, in press.
[47] A.T. Dinsdale, SGTE data for pure elements, Calphad 15 (1991) 317–425.
[48] J.O. Andersson, A.F. Guillermet, M. Hillert, B. Jansson, B. Sundman, A compound-energy model of ordering in a phase with sites of different coordination numbers, Acta Met. 34 (1986) 437–445.
[49] M. Hillert, The compound energy formalism, J. Alloy. Compd. 320 (2001) 161–176.
[50] R. Schmid-Fetzer, S.-M. Liang, Thermodynamic assessment of the Al–Cu–Zn system, part III: Al–Cu–Zn ternary system, Calphad (2015) (in prepration).
[51] W. Cao, S.L. Chen, F. Zhang, K. Wu, Y. Yang, Y.A. Chang, R. Schmid-Fetzer, W. A. Oates, PANDAT software with PanEngine, PanOptimizer and PanPrecipitation for multi-component phase diagram calculation and materials property simulation, Calphad 33 (2009) 328–342.